Influence of wheel-polygonal wear on the dynamic forces within the axle-box bearing of a high-speed train

Zhiwei Wang, Paul Allen, Guiming Mei, Ruichen Wang, Huizhong Yin, Weihua Zhang

Zhiwei Wang, tpl_zw@163.com, State Key Laboratory of Traction Power, Southwest Jiaotong University, Chengdu, Sichuan 610031, China.

Paul Allen, p.d.allen@hud.ac.uk, Institute of railway research, University of Huddersfield, Huddersfield, HD1 3DH, UK.

Guiming Mei, **corresponding author**, 13880068468@163.com, State Key Laboratory of Traction Power, Southwest Jiaotong University, Chengdu, Sichuan 610031, China.

Ruichen Wang, R.Wang@hud.ac.uk, Institute of railway research, University of Huddersfield, Huddersfield, HD1 3DH, UK.

Zhonghui Yin, 15802874801@163.com, State Key Laboratory of Traction Power, Southwest Jiaotong University, Chengdu, Sichuan 610031, China.

Weihua Zhang, tpl@home.swjtu.edu.cn, State Key Laboratory of Traction Power, Southwest Jiaotong University, Chengdu, Sichuan 610031, China.

Abstract

The axle-box bearing is a key component of a high-speed train, providing a safety-critical load path for axial and radial forces transmitted between the wheel-rail interface and the bogie frame. Failure of axle-box bearings can directly affect operational and safety performance of the train, and therefore understanding their operating state is key to predicting potential failure modes and planning maintenance interventions.

In this study, a three-dimensional vehicle-track coupled dynamics model, with the inclusion of the axle-box bearings has been developed. Based on the bearing's structural properties and operating characteristics, the coupling effects of the vehicle components relative to the bearing are considered. The model also takes a number of non-linear factors into account, such as time-varying bearing stiffness, bearing clearance, wheel-polygonal wear and the non-linear wheel-rail contact forces. Dynamic analysis of the model has been carried out through numerical simulations that consider different amplitudes and harmonic orders of measured and idealised polygonal wheel wear. Both model analysis and validation was supported by field tests performed on a high-speed rail line. Simulation results show that the amplitude of rolling contact forces of the axle-box bearing increases with vehicle speed and the amplitude of polygonal wear. However, the influence of wear upon the axle-box bearing is found to be small in the low-speed range, but at higher operating speeds, polygonal wear begins to lead to a rapid increase in bearing contact forces and the potential for degradation. As a result of vehicle operations, both high order (17^{th} to 20^{th} order) and lower order (1^{st} to 4^{th} order) wheel polygonal wear patterns are generated. The former's influence on axle-box bearing forces is more significant. Hence, the identification and rectification of this order of wear should form part of maintenance practice and potentially also be considered in the design of axle-box bearings for high-speed trains.

Keywords: Axle-box bearing, vehicle-track coupled dynamics, wheel polygonal wear, contact force,

high-speed train.

1 Introduction

High-speed trains in China have developed rapidly in recent years. With an increase in the use of such trains, problems such as wheel polygonal wear, cracking of the gearbox housing and failure of the axle-box bearing are emerging. The axle-box bearing is a key component, offering a high load capacity against both axial and radial loads. The dynamic performance of the axle-box bearing directly affects the operational safety, in severe cases, bearing failure can lead to train derailment and potentially serious accidents.

Polygonal wear is a common form of uneven wear in the circumferential direction of high-speed train wheels during operation, also referred to as out-of-round. Previous research [1] has shown that such wear can result in high frequency wheel-rail impact loads, which are detrimental to ride quality and wheel-rail asset life. Moreover, the frequency of the impact loads increases with the order of polygonal wear and running speed. Hence, the impact loads caused by polygonal wear can result in wheel-rail noise [2] and fatigue problems for the vehicle-track components [3]. A number of previous studies have focused on the mechanism leading to polygonal wear [4] and its influence on noise and the dynamic performance [5] of the wheel-rail system.

Experiments and simulations have been conducted to investigate the effects of the wheel polygonal wear. Johansson and Nielsen [6] investigated the effects of out-of-round wheels upon the dynamic wheel-rail contact force and track response. It was found that wheel defects may induce excessive wheel-rail forces, resulting in damage to the wheel-rail system. The impact of wheel flatness upon the dynamic response of high-speed trains was investigated by Zhai [7]; Liu and Zhai [8] whom studied the vertical dynamic performance of the wheel-rail force with a polygonal wheel, by means of a coupled vertical-dynamics model of the vehicle-track system. The study concluded that the dynamic wheel-rail load is more sensitive to high order harmonics at increased speeds, and that the short-wavelength components of the polygonal wheel can stimulate high frequency vibration of the track. Meanwhile, the influence of polygonal wear upon static and dynamic imbalances, using a dynamic model based on flexible deformation of the wheelset was invested by Meinke [9]. Zhiwei Wang [10, 11] studied the dynamic performance of a gearbox housing under the effect of wheel polygonal wear. Xingwen Wu [12, 13] investigated the effects of polygonal wear and wheel flats on the wheelset using a coupled vehicle-track dynamics model including a flexible wheelset. It was concluded that polygonal wear of the wheel can lead to significantly higher vibration and stress than that of a healthy wheelset.

Most investigations have focused on the mechanism of polygonal wear and its influence upon the dynamic performance of the wheel-rail system; however, little attention has been paid to the dynamic performance of the axle-box bearing when subject to such wear. The dynamic performance of tapered roller bearings (TRBs) without consideration of the coupling effects of the vehicle has attracted significant research effort. Palmgren [14], Jones [15] and Harris [16] introduced fundamental theories of rolling bearings. Andreason [17] investigated the load distribution of TRBs with both radial and axial loads. Liu [18] improved the model proposed by Andreason and investigated the effect of misalignment under combined loads. Based on previous studies, Houpert [19] developed an analytical approach for determining the loads and moments of TRBs as a function of the given displacement when considering the transition from point to line contact between rollers

and raceways with increasing load. Jing Liu [20] investigated the dynamic characteristics of a TRB under a surface fault, via a simplified model considering the contact forces between the roller and raceways. Recently, Zhiwei Wang [21] investigated TRB dynamics performance considering the coupling effects of the vehicle-track system, which established a simplified dynamics model of TRBs, that concluded the vibration environment of the axle-box bearing cannot be ignored in such studies.

Previous work on axle-box bearings have typically failed to consider the coupling effects of the vehicle-track system; i.e., the dynamic interactions between the axle-box bearing and the traditional vehicle-track system are often neglected. In practice, the TRBs of the axle-box interact dynamically with the connected components of high-speed trains. Some authors realised that it is important to couple the vehicle and track together due to the intensified wheel-rail interactions as the train's running speed increases [22, 23], especially if wheel defects occur [11,12]. Moreover, the vibration of vehicle components is significantly influenced by wheel polygonal wear and likewise the life of the bearing is directly related to its dynamic load environment [24].

This paper aims to develop a vehicle-track coupled dynamics model to investigate the effect of polygonal wear upon the dynamic performance of axle-box bearings. Here the coupled effects from the vibrations of the vehicle components upon the axle-box bearing are included, based on classical vehicle-track coupled dynamics theory and that of the TRB's dynamics. And, the interactions between the roller and the raceway, and guiding flange are modelled in detail. Based on this model, the dynamic response of the vehicle-track system is calculated under excitations of polygonal wheel wear and non-linear factors, including the time-varying stiffness of the bearing and the clearance of the TRBs. Field tests on the Beijing–Shanghai high-speed rail line are also performed to help analyse and validate the developed dynamic model. Furthermore, the influence of the amplitude and the order of wheel polygonal wear on dynamic performance of the axle-box bearing are investigated in detail.

2 Three-dimensional vehicle-track coupled dynamics model

A three-dimensional vehicle-track coupled dynamics model is the foundation of this study. During the last decade, different types of vehicle-track system models have been established for various research purposes. In this paper, a new vehicle-track coupled dynamics model with the inclusions of an axle-box bearing is presented. By including a detailed bearing model, the work represents a clear development of previous studies [25].

Figure 1–Figure 2 illustrate the details of the vehicle-track coupled dynamics model, including the vehicle subsystem, the axle-box bearing subsystem, the rail subsystem and the wheel-rail relationship describing the interaction between the vehicle and the rail.

The vehicle consists of a car body, two bogie frames, four wheelsets and eight axle-boxes. The car body is supported on two bogies via secondary suspensions at each end and the bogie frames are connected to the wheelsets via a primary suspension system. The primary and secondary suspensions are modelled as parallel combinations of the equivalent spring and viscous dampers, along the three translational directions. Moreover, yaw dampers and anti-roll bars are considered in the secondary suspensions. The model of the axle-box bearing is described in the section 'Non-

linear force on the axle-box bearing'. In the vehicle subsystems, the axle-box has three translational degrees of freedom (DOFs), while the other components have five DOFs. The resultant trailer car sub-model has 59 DOFs in total, as shown in Table 1.

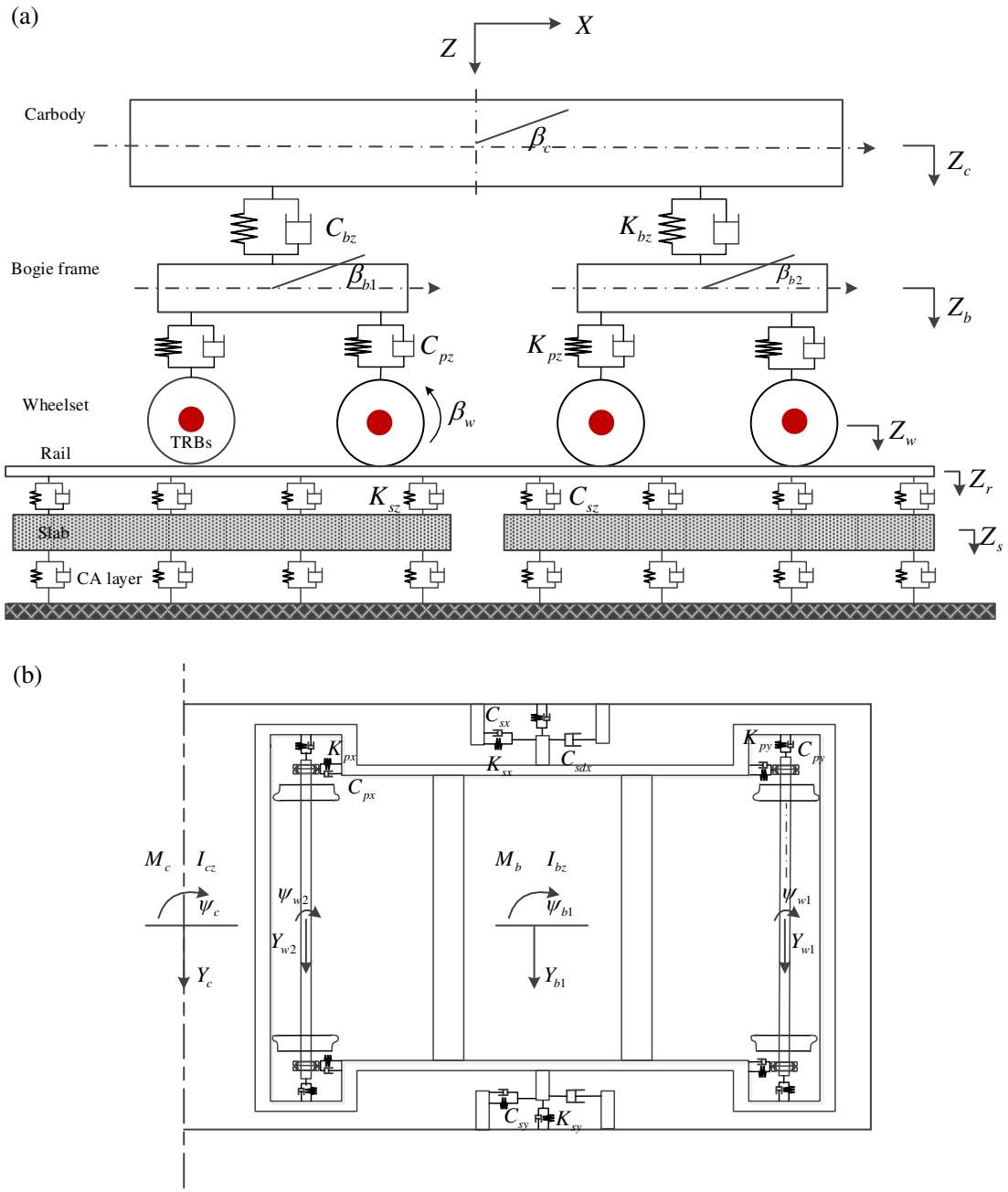

Figure 1 Three-dimensional vehicle-track coupled dynamics model : (a) elevation and (b) plan view

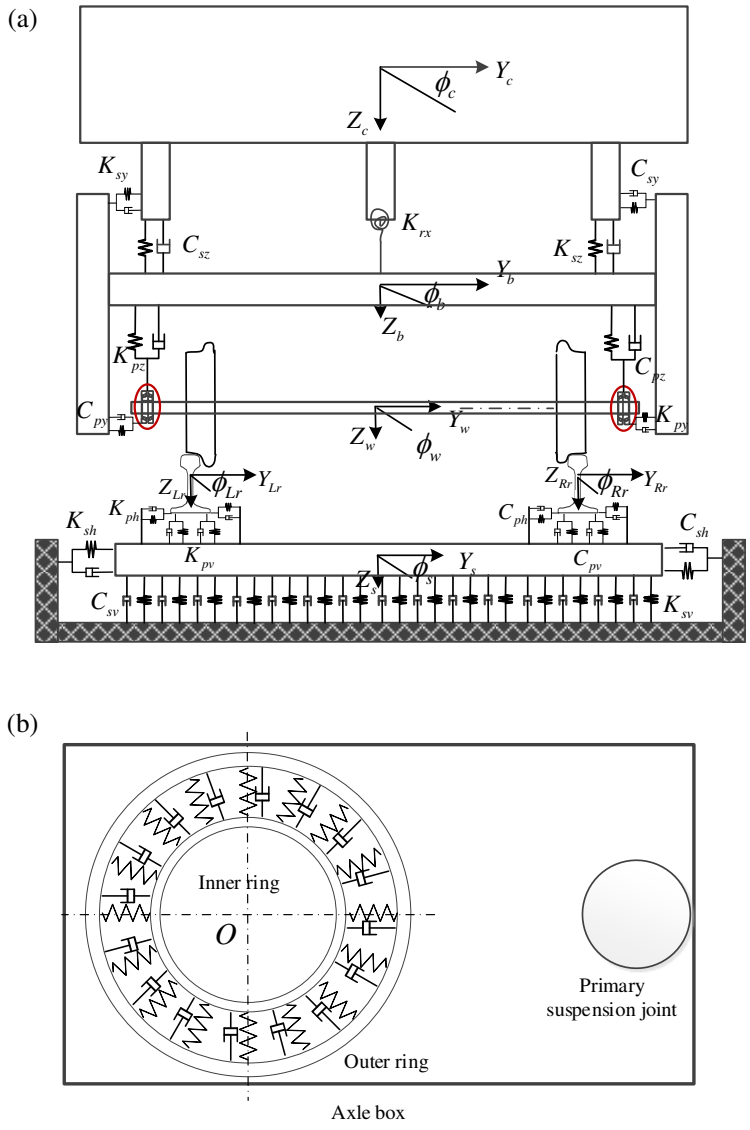

Figure 2 Three-dimensional vehicle-track coupled dynamics model (end view)

In this investigation, a typical slab-track structure is employed, including the rail, rail pads, slabs and subgrade, as shown in Figure 1 and Figure 2 (a). Both the left and right rails are treated as Timoshenko beams with motions in the vertical, lateral and torsional directions, which are supported by slabs. The established three-dimensional slabs are described as elastic rectangular plates supported on a viscoelastic foundation. K_{sv} and C_{sv} are the vertical stiffness and damping of the CA layer, respectively, while K_{sh} and C_{sh} are their lateral counterparts. The parameters are detailed in Section 3. Because the lateral bending stiffness of the slab is very large, it is sufficient to consider the rigid mode of slab vibration in the lateral direction. The slab-track sub-model equations are solved by the modal-superposition method, which has been well documented in [22] and is therefore not introduced here.

Regarding the wheel-rail interactions, the normal force between the wheel and the rail is calculated using the non-linear Hertzian elastic contact theory [22, 26], which is employed commonly in investigations of wheel-rail interactions. The tangential wheel-rail contact forces were estimated using the Shen–Hedrick–Elkins model [27], which is based on Kalker's linear creep theory [28]. The wheel-rail coupling model has been well documented in [29], so its details are neglected in this

paper.

Table 1 Degrees of freedom of the high-speed vehicle dynamic model

Vehicle component	Lateral motion	Vertical motion	Roll motion	Yaw motion	Pitch motion
Car body	Y_{c}	Z_{c}	ϕ_{c}	ψ_{c}	β_{c}
Bogie frame (i =1,2)	$Y_{\mathrm{b}i}$	$Z_{\mathrm{b}i}$	$\phi_{\mathrm{b}i}$	$\psi_{\mathrm{b}i}$	$\beta_{\mathrm{b}i}$
Axle-box (i =1–8)	Y_{ai}	Z_{ai}			
Wheelset (i =1–4)	$Y_{\mathrm{w}i}$	$Z_{\mathrm{w}i}$	$\phi_{\mathrm{w}i}$	$\psi_{\mathrm{w}i}$	$\beta_{\mathrm{w}i}$

(Notes: Besides the DOFs of the table, the longitudinal motion of axle-box is taken into consideration.)

2.1 Internal forces of the vehicle subsystem

In the three-dimensional vehicle-track coupled dynamics model, the interactions between the lumped masses are performed by the spring-damper elements. Comparing to the classical three-dimensional vehicle-track coupled dynamics model, the axle-box subsystem provides the novel element, allowing the dynamic state of the double-row tapered roller bearing to be analysed in detail during operation. As the secondary suspension forces of the vehicle system are the same as the classical model [30], the expressions of the forces between the car body and the bogie are not presented here. The axle-box subsystem is coupled with the wheelset and bogie, which is not considered in the classical vehicle-track coupled dynamics model, the expressions of the primary suspension force are demonstrated as below.

The primary longitudinal-spring and damping forces between the axle-box and the bogie are:

$$\begin{cases} F_{\mathrm{xfL}i} = K_{\mathrm{px}}\left(d_{\mathrm{w}}\psi_{\mathrm{b}n} + H_{\mathrm{bw}}\beta_{\mathrm{b}n} - X_{\mathrm{aL}i}\right) \\ \qquad + C_{\mathrm{px}}\left(d_{\mathrm{w}}\dot{\psi}_{\mathrm{b}n} + H_{\mathrm{bw}}\dot{\beta}_{\mathrm{b}n} - \dot{X}_{\mathrm{aL}i}\right) \\ F_{\mathrm{xfR}i} = K_{\mathrm{px}}\left(-d_{\mathrm{w}}\psi_{\mathrm{b}n} + H_{\mathrm{bw}}\beta_{\mathrm{b}n} - X_{\mathrm{aR}i}\right) \\ \qquad + C_{\mathrm{px}}\left(-d_{\mathrm{w}}\dot{\psi}_{\mathrm{b}n} + H_{\mathrm{bw}}\dot{\beta}_{\mathrm{b}n} - \dot{X}_{\mathrm{aR}i}\right) \end{cases} \quad (i = 1,2,3,4) \tag{1},$$

While the primary lateral-spring and damping forces between the axle-box and the bogie can be calculated as follows:

$$\begin{aligned} F_{y\mathrm{f(L,R)}i} = {} & K_{\mathrm{py}}\left(Y_{\mathrm{a(L,R)}i} - Y_{\mathrm{b}n} + H_{\mathrm{bw}}\phi_{\mathrm{b}i} + (-1)^{i} l_{\mathrm{b}}\psi_{\mathrm{b}n}\right) \\ & + C_{\mathrm{py}}\left(\dot{Y}_{\mathrm{a(L,R)}i} - \dot{Y}_{\mathrm{b}n} + H_{\mathrm{bw}}\dot{\phi}_{\mathrm{b}n} + (-1)^{i} l_{\mathrm{b}}\dot{\psi}_{\mathrm{b}n}\right) \qquad (i = 1,2,3,4) \end{aligned} \tag{2}.$$

Finally, the primary vertical-spring and damping forces between the axle-box and the bogie are given by:

$$\begin{cases} F_{z\mathrm{fL}i} = K_{\mathrm{pz}}\left(Z_{\mathrm{b}n} - Z_{\mathrm{aL}i} + (-1)^{i} l_{\mathrm{b}}\beta_{\mathrm{b}n} - d_{\mathrm{w}}\phi_{\mathrm{b}n}\right) \\ \qquad + C_{\mathrm{pz}}\left(\dot{Z}_{\mathrm{b}n} - \dot{Z}_{\mathrm{aL}i} + (-1)^{i} l_{\mathrm{b}}\dot{\beta}_{\mathrm{b}n} - d_{\mathrm{w}}\dot{\phi}_{\mathrm{b}n}\right) \\ F_{z\mathrm{fR}i} = K_{\mathrm{pz}}\left(Z_{\mathrm{b}n} - Z_{\mathrm{aR}i} + (-1)^{i} l_{\mathrm{b}}\beta_{\mathrm{b}n} + d_{\mathrm{w}}\phi_{\mathrm{b}n}\right) \\ \qquad + C_{\mathrm{pz}}\left(\dot{Z}_{\mathrm{b}n} - \dot{Z}_{\mathrm{aR}i} + (-1)^{i} l_{\mathrm{b}}\dot{\beta}_{\mathrm{b}n} + d_{\mathrm{w}}\dot{\phi}_{\mathrm{b}n}\right) \end{cases} \quad (i = 1,2,3,4) \tag{3}.$$

2.2 Non-linear forces on the axle-box bearing

The motion and interaction between the components of the axle-box bearings are complex; in this paper, a model considering the interactions between the bearing rolling elements and inner and outer raceways and guiding flanges is developed. When subjected to external loads imparted by the bogie and those generated within wheel-rail contact, the forces of the roller-inner/outer raceway and the contact load of roller-guiding flange are required to react these. The theoretical analysis is based on the following assumptions [28]: the friction between the internal components of bearing are ignored, the effects of lubrication is not considered, the motion between rollers and raceways maintains pure rolling without slip.

From the force diagram of the TRBs shown in Figure 3, the equilibrium equations can be obtained as outlined below:

$$\begin{cases} Q_{\mathrm{e}} \sin\alpha_{\mathrm{e}} - Q_{\mathrm{i}} \sin\alpha_{\mathrm{i}} - Q_{\mathrm{f}} \sin\alpha_{\mathrm{f}} = 0 \\ Q_{\mathrm{e}} \cos\alpha_{\mathrm{e}} - Q_{\mathrm{i}} \cos\alpha_{\mathrm{i}} + Q_{\mathrm{f}} \cos\alpha_{\mathrm{f}} - F_{\mathrm{c}} = 0 \end{cases} \tag{4}$$

where Q_{i} and Q_{e} is the contact force between roller and inner and outer raceway, respectively. Q_{f} is the contact force between the outer end of the tapered roller and guiding flange of the inner ring. F_{c} is the centrifugal force, α_{i} , α_{e} and α_{f} is the contact angle of the roller-inner raceway, roller-outer raceway and roller-guiding flange, respectively.

The centrifugal force of roller can be determined by:

$$F_{\mathrm{c}} = \frac{1}{2} m d_{\mathrm{m}} \omega_{\mathrm{c}}^2 \tag{5}$$

where m is the mass of roller, d_{m} is the pitch diameter of double-row tapered roller bearing, ω_{c} is the orbital angular velocity of rollers, and it can be obtained by:

$$\omega_{\mathrm{c}} = \frac{\omega_{\mathrm{i}}}{2d_{\mathrm{m}}} \left(d_{\mathrm{m}} - D_{\mathrm{b}} \cos\frac{\alpha_{\mathrm{i}} + \alpha_{\mathrm{e}}}{2} \right) \tag{6}$$

Where ω_{i} is the rotating speed of inner ring. D_{b} is the average diameter of tapered roller.

(a) (b)

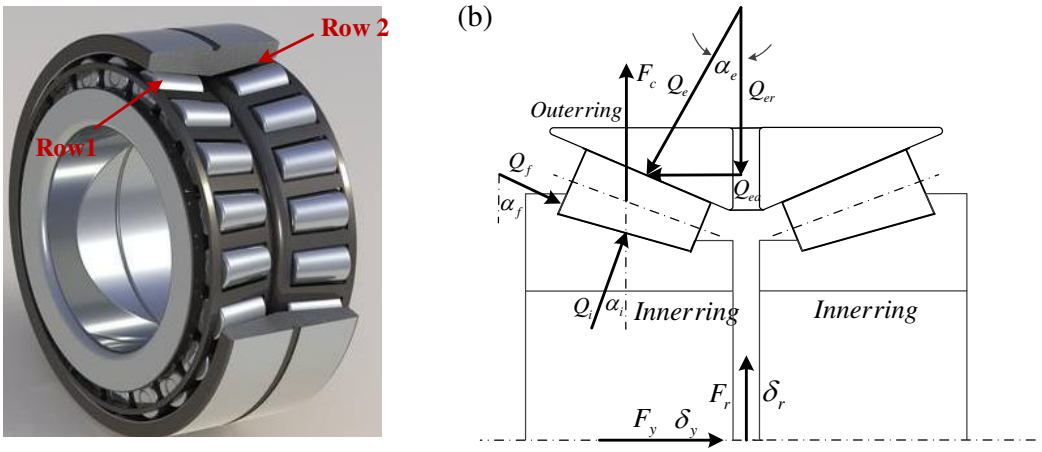

Figure 3 Double row tapered roller bearing

Within the model, there is a contact force Q_{e} with respect to the outer ring only. Hence, the roller-inner ring of the double-row TRBs can be considered as an isolated body for mechanical analysis [31]. In this way, it is only necessary to super-impose the contact force components of the roller-outer raceway for each roller in the radial and axial directions to derive the reaction forces to external loads. Furthermore, the contact forces of the roller-inner ring raceway and the contact forces

between the outer end of the tapered roller and guiding flange of inner ring can be obtained by equation (4).

As presented in Figure 3, when the bearing has radial and axial displacements, and considering the initial clearance (g_{h}) in the radial direction, the total compression at any roller azimuthal location ψ_j can be determined as [21]

$$\delta_{1ej} = [\delta_{\mathrm{r}} \cos\psi_j - 0.5\,\mathrm{g_h}(1-\cos\psi_j)]\cos\alpha_{\mathrm{e}} + \delta_y \sin\alpha_{\mathrm{e}} \quad (j = 1-21) \tag{7},$$

$$\delta_{2ej} = [\delta_{\mathrm{r}} \cos\psi_j - 0.5\,\mathrm{g_h}(1-\cos\psi_j)]\cos\alpha_{\mathrm{e}} - \delta_y \sin\alpha_{\mathrm{e}} \quad (j = 1-21) \tag{8},$$

where δ_{1ej} and δ_{2ej} are the total compression along the normal direction of the outer raceway contact line of the two bearings, δ_{r} and δ_y are the radial and axial displacements (respectively) of the inner ring relative to outer ring. The inner ring of the axle-box bearing rotates with the wheelset, the roller azimuthal location ψ_j can be described using the cage rotation speed ω_{c} as:

$$\psi_j = \frac{2\pi}{N_j}(j-1) + \omega_{\mathrm{c}} t \tag{9},$$

The radial displacement δ_{r} can be calculated using the expression:

$$\delta_{\mathrm{r}} = \sqrt{\delta_x^2 + \delta_z^2} \tag{10}.$$

where δ_x and δ_z are the longitudinal and vertical displacements of the inner ring relative to outer ring, respectively. And then, the total contact force between the roller and outer raceway can be obtained by:

$$Q_{mej} = K_{me}\delta_{mej}^{1.11} \tag{11}$$

Where K_{me} is total contact stiffness coefficient between roller and outer raceway, which can be determined by [32]:

$$K_{me} = 6.24\times10^4 l_{\mathrm{e}}^{0.84} D_b^{0.11}[1 + \mathrm{c_i^{0.9}}\cos(\alpha_{\mathrm{e}} - \alpha_{\mathrm{i}})] \tag{12}$$

Where l_{e} is the effective contact length, c_{i} is an index, which can be obtained by:

$$c_{\mathrm{i}} = \sin(\alpha_{\mathrm{e}} - \alpha_{\mathrm{i}}) / \sin(\alpha_{\mathrm{i}} + \alpha_{\mathrm{f}}) \tag{13}$$

By substituting equations (7) and (8) into equation (11), the contact force of each roller can be calculated as follows:

$$Q_{mej} = \begin{cases} K_{me}\delta_{mej}^{10/9} & \delta_{mej} > 0 \\ 0 & \delta_{mej} < 0 \end{cases} \quad (j = 1-21) \tag{14},$$

where the row number of the bearings is m = 1,2. Based on the analysis above and the literatures results [20, 21], the resultant forces of each axle-box bearing are as follows:

$$\begin{cases} F_{xa} = \sum_{m=1}^{2}\sum_{j=1}^{21} Q_{mej}\cos\alpha_{\mathrm{e}}\cos\psi_{mj}\cos(\arctan(\frac{\delta_z}{\delta_x})) + C_{\mathrm{a}}(\dot{X}_{\mathrm{a}} - \dot{X}_{\mathrm{w}} - \dot{\psi}_{\mathrm{w}} a_0) \\ F_{\mathrm{ya}} = \sum_{m=1}^{2}\sum_{j=1}^{21} Q_{mej}\sin\alpha_{\mathrm{e}} + C_a(\dot{Y}_a - \dot{Y}_w) \\ F_{\mathrm{za}} = \sum_{m=1}^{2}\sum_{j=1}^{21} Q_{mej}\cos\alpha_{\mathrm{e}}\cos\psi_{mj}\sin(\arctan(\frac{\delta_z}{\delta_x})) + \mathrm{C_a}\left(\dot{Z}_{\mathrm{a}} - \dot{Z}_{\mathrm{w}} - \dot{\phi}_{\mathrm{w}} a_0\right) \end{cases} \tag{15}.$$

Where C_{a} is the damping coefficient in the TRBs. The relative displacement in each roller's angular position between the inner and outer raceway can be obtained, which is coupled with the movement of wheelset and axle-box, and has been well documented in [21]. Therefore, a detailed

description of the displacement relationship of TRBs is not presented here.

2.3 Equations of motion

The equations of motion of the vehicle model consist of one car body, two bogie frames, four wheelsets and corresponding axle-boxes. The motion equations of the car body and bogie frame are not described here as they follow classical vehicle-track coupled dynamics. However, the equations of motion of the axle-box and wheelset are improved over classical theory, hence the details of the governing equations are described in detail below.

(1) The equations of motion of the axle-box

longitudinal motion:

$$M_{\mathrm{a}}\ddot{X}_{\mathrm{a(L,R)i}} = F_{xf(\mathrm{L,R})i} - F_{xa(\mathrm{L,R})i} \qquad (i=1,2,3,4) \tag{16};$$

lateral motion:

$$M_{\mathrm{a}}\ddot{Y}_{\mathrm{a(L,R)}i} = -F_{yf(\mathrm{L,R})i} + F_{ya(\mathrm{L,R})i} \qquad (i=1,2,3,4) \tag{17};$$

bounce motion:

$$M_{\mathrm{a}}\ddot{Z}_{\mathrm{a(L,R)i}} = F_{zf(\mathrm{L,R})\mathrm{i}} - F_{za(\mathrm{L,R})i} \qquad (i=1,2,3,4) \tag{18}.$$

(2) The equations of motion of the wheelset

lateral motion:

$$M_{\mathrm{w}}\ddot{Y}_{\mathrm{w}i} = -F_{\mathrm{yaL}i} - F_{\mathrm{yaR}i} + F_{\mathrm{L}yi} + F_{\mathrm{R}yi} + N_{\mathrm{L}yi} + N_{\mathrm{R}yi} \qquad (i=1,2,3,4) \tag{19};$$

bounce motion:

$$M_{\mathrm{w}}\ddot{Z}_{\mathrm{w}i} = -F_{\mathrm{L}zi} - F_{\mathrm{R}zi} - N_{\mathrm{L}zi} - N_{\mathrm{R}zi} + F_{\mathrm{zaL}i} + F_{\mathrm{zaR}i} \qquad (i=1,2,3,4) \tag{20};$$

roll motion:

$$\begin{aligned} I_{\mathrm{w}x}\ddot{\phi}_{\mathrm{w}i} - I_{\mathrm{w}y}(\dot{\beta}_{\mathrm{w}i} - \Omega)\dot{\psi}_{\mathrm{w}i} = {} & a_0\left(F_{\mathrm{L}zi} + N_{\mathrm{L}zi} - F_{\mathrm{R}zi} - N_{\mathrm{R}zi}\right) - r_{\mathrm{L}i}\left(F_{\mathrm{L}yi} + N_{\mathrm{L}yi}\right) \\ & - r_{\mathrm{R}i}\left(F_{\mathrm{R}yi} + N_{\mathrm{R}yi}\right) + d_{\mathrm{w}}(F_{\mathrm{zaR}i} - F_{\mathrm{zaL}i}) \qquad (i=1,2,3,4) \end{aligned} \tag{21};$$

rotational motion:

$$\begin{aligned} I_{\mathrm{w}y}\ddot{\beta}_{\mathrm{w}i} = {} & r_{\mathrm{R}i}F_{\mathrm{R}xi} + r_{\mathrm{L}i}F_{\mathrm{L}xi} + r_{\mathrm{R}i}\psi_{\mathrm{w}i}(F_{\mathrm{R}yi} + N_{\mathrm{R}yi}) \\ & + r_{\mathrm{L}i}\psi_{\mathrm{w}i}\left(F_{\mathrm{L}yi} + N_{\mathrm{L}yi}\right) + M_{\mathrm{L}yi} + M_{\mathrm{R}yi} + N_{\mathrm{L}xi}r_{\mathrm{L}i} + N_{\mathrm{R}xi}r_{\mathrm{R}i} \qquad (i=1,2,3,4) \end{aligned} \tag{22};$$

yaw motion:

$$\begin{aligned} I_{\mathrm{w}z}\ddot{\psi}_{\mathrm{w}i} - I_{\mathrm{w}y}\dot{\phi}_{\mathrm{w}i}\left(\dot{\beta}_{\mathrm{w}i} - \Omega\right) = {} & a_0(F_{\mathrm{L}xi} - F_{\mathrm{R}xi}) + a_0\psi_{\mathrm{w}i}\left(F_{\mathrm{L}yi} + N_{\mathrm{L}yi} - F_{\mathrm{R}yi} + N_{\mathrm{R}yi}\right) \\ & + M_{\mathrm{L}zi} + M_{\mathrm{R}zi} + d_{\mathrm{w}}(F_{\mathrm{xaL}i} - F_{\mathrm{xaR}i}) \\ & + a_0(N_{\mathrm{L}xi} - N_{\mathrm{R}xi}) \qquad (i=1,2,3,4) \end{aligned} \tag{23}.$$

In equations (16)–(23), the vibrations of the vehicle components are coupled together. This comprehensive vehicle-track dynamics model enables more realistic dynamic simulations of the axle-box bearing under conditions such as wheel-polygonal wear, wheel flats and track defects.

2.4 Wheel-polygonal model

To investigate the influence of polygonal wheel wear upon the axle-box bearings, an idealised polygonal wear pattern is adopted. The wheel polygon is generated by changing the radius of the wheel's rolling cycle, while the harmonic function is used to simulate the change in this radius. The

relevant equations are as follows:

$$\begin{cases} \Delta r = A\sin(N\beta + \beta_0) \\ r(\beta) = \mathrm{R} - \Delta r \end{cases} \tag{24}$$

where A is the magnitude of polygonal wear, N is the order of the polygonal wheel, β is the angle of wheel rotation, β_0 is the phase angle, Δr is the wheel-diameter difference along its circumference and R is the nominal rolling radius of the wheel. Different polygonal wheels can be simulated by modifying the order and magnitude of the wheel-polygonal wear.

3 Numerical simulation and analysis of results

Based on the established vehicle-track coupled dynamics model, the dynamic response of the complete system, including the vehicle, axle-box, the axle-box bearing and the track subsystems is obtained for a high-speed train running on straight track. The key parameters of the vehicle subsystems used for the simulations are presented in Table 2. Moreover, the parameters of the slab track employed in [33] are adopted. At the same time, the corresponding vibrational data is obtained from field test. The structural parameters of the axle-box bearing are provided in Table 3.

Table 2 Main parameters of the vehicle model

Notation	Specification	Value
M_c	Car body mass (10^3 kg)	38.9
M_b	Bogie frame mass (kg)	2200
M_w	Wheelset mass (kg)	1517
M_a	Axle-box mass (kg)	66.7
I_{cx} / I_{cy} / I_{cz}	Mass moment of car body about x/y/z axes (10^3 kg/m^2)	126/1905/1798
I_{bx} / I_{by} / I_{bz}	Mass moment of bogie frame about x/y/z axes (kg/m^2)	1236/1233/2336
I_{wx} / I_{wy} / I_{wz}	Mass moment of wheelset about x/y/z axes (kg/m^2)	693/118/693
K_{sx} / K_{sy} / K_{sz}	Stiffness of secondary suspension along x/y/z (10^3 N/m)	133/133/203
C_{sx} / C_{sy} / C_{sz}	Damping of secondary suspension along x/y/z (10^3 N s/m)	10.4
K_{px} / K_{py} / K_{pz}	Stiffness of primary suspension along x/y/z (10^3 N/m)	920/920/940
C_{pz}	Damping of primary suspension along z (10^3 N s/m)	10
H_{cB}	Vertical distance between car body centroid and top of secondary suspension (m)	0.738
H_{Bt}	Vertical distance between bogie frame centroid and bottom of secondary suspension (m)	0.06
H_{bw}	Vertical distance between bogie frame centroid and wheelset centerline (m)	0.06
d_s	Semi-lateral distance between secondary suspension (m)	0.95
d_{sc}	Semi-lateral distance between yaw damper (m)	1.275
d_w	Semi-lateral distance between primary suspension (m)	1.0
l_c	Semi-longitudinal distance between bogies (m)	8.6875
l_b	Semi-longitudinal distance between wheelsets in bogie (m)	1.25

Table 3 Structure parameters of axle-box bearing of a high-speed train

Structure parameters	value
The average diameter of roller (D_b /mm)	23
The contact angle of roller-inner raceway (α_i /degree)	7.75
The contact angle of roller-inner raceway (α_e /degree)	10
The effective length of roller (l_e /mm)	45
The pitch diameter of the bearing (d_m /mm)	180.5
Number of rollers in each row (z)	21

3.1 Field test and model validation

To validate the dynamic model, experimental field tests were carried out along the Beijing–Shanghai high-speed rail line. Vibrational data was acquired separately from the bogie frame and the axle-box, the position of vibration-data acquisition is shown in Figure 4. The acceleration data was collected in both the lateral and vertical directions with a sampling frequency of 5000 Hz.

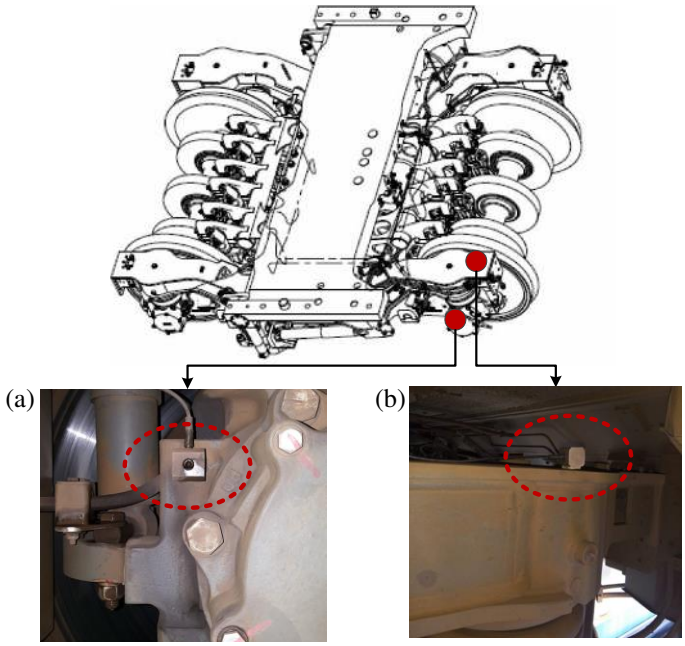

Figure 4 Monitoring positions. (a) The accelerator sensor on axle-box and (b) bogie frame.

Wheel wear measurements we taken during the period of October 2016 and March 2017, a total of 1056 wheel profile measurements were recorded for the same vehicle type prior to re-profiling. Polygonal wear patterns were observed on all of the measured wheels. The profiles were measured around the complete wheel circumference with a resolution of 1mm using a BBM wheel roughness measuring device at the rolling circle of the wheel, as shown in Figure 5 (a). Profile data was recorded with an accuracy of 0.1 μm .

The proportion of different harmonic orders of wheel polygonal wear for all measured wheels is shown in Figure 5 (b) and (c). It is clear that two types of wheel polygonal wear predominantly occurs; namely low order wheel polygonal wear, as per Figure 5 (b), and high order wheel polygonal wear, as shown in Figure 5 (c). Referring to Figure 5 (b), it can be concluded that the proportion of 1st order wheel polygonal wear is the highest, this is related to eccentricity of the wheel's mass from the centre of rotation, together with deficiencies in manufacturing or maintenance processes. The 2nd to 4th order wheel polygonal wear accounts for only 12.6% of the data set. The statistical results

of high harmonic order wheel polygonal wear show that 20th order wear is the most prominent followed by 19th order. Therefore, the most predominant orders of wheel polygonal identified above will form the focus of more detailed analysis.

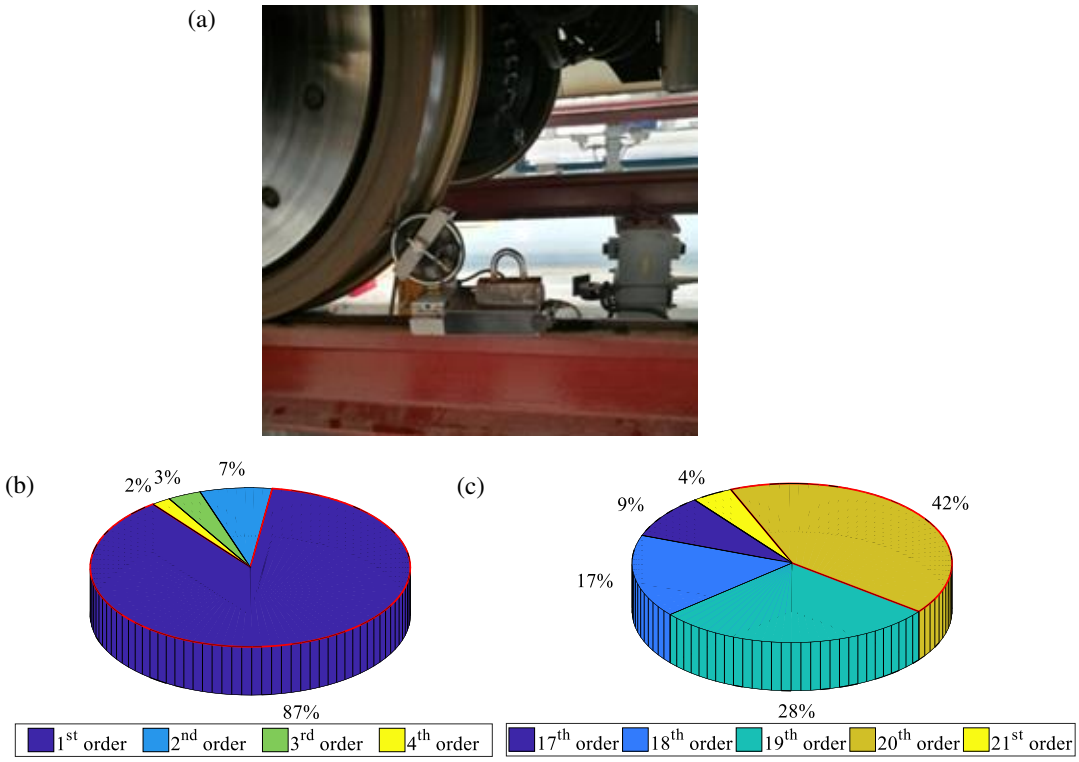

Figure 5 Wheel polygonal wear measurements: (a) the wheel roughness measuring device, proportion of (b) the low harmonic orders and (c) the high harmonic orders.

The 20th order wheel polygonal wear was found to be the most common high order form of wear, the associated measured wheel shapes are shown in Figure 6. Figure 6 (a), (b) and (c), respectively, indicate polygonal wear in the Cartesian coordinate system, the polar coordinate system, together with the irregularity spectrum of the polygonal wear. The maximum amplitude of wear is approximately 0.08 mm, as shown in Figure 6 (a). In addition, according to the irregularity spectrum in Figure 6 (c), the wheel typically shows 1st and 20th order polygonal wear.

To compare the dynamic responses due to wheel polygonal wear for calculation and experimental results, numerical simulations are performed using the developed vehicle-track dynamics model using the measured 20th order polygonal shape (Figure 6). Time histories and the corresponding spectrum acquired from the bogie frame and the axle-box at a speed of 300 km/h are presented in Figure 7 and 8, along with the corresponding numerical simulation results.

In Figure 7 (a), the vibrations of the bogie frame acquired during field tests are slightly larger than the theoretical results. This is due to the high-frequency vibration of the bogie frame, which due to the rigid body approach could not be fully represented in the dynamic model. However, the model captures the majority of the key dynamic-vibration characteristics of the bogie frame required for this study.

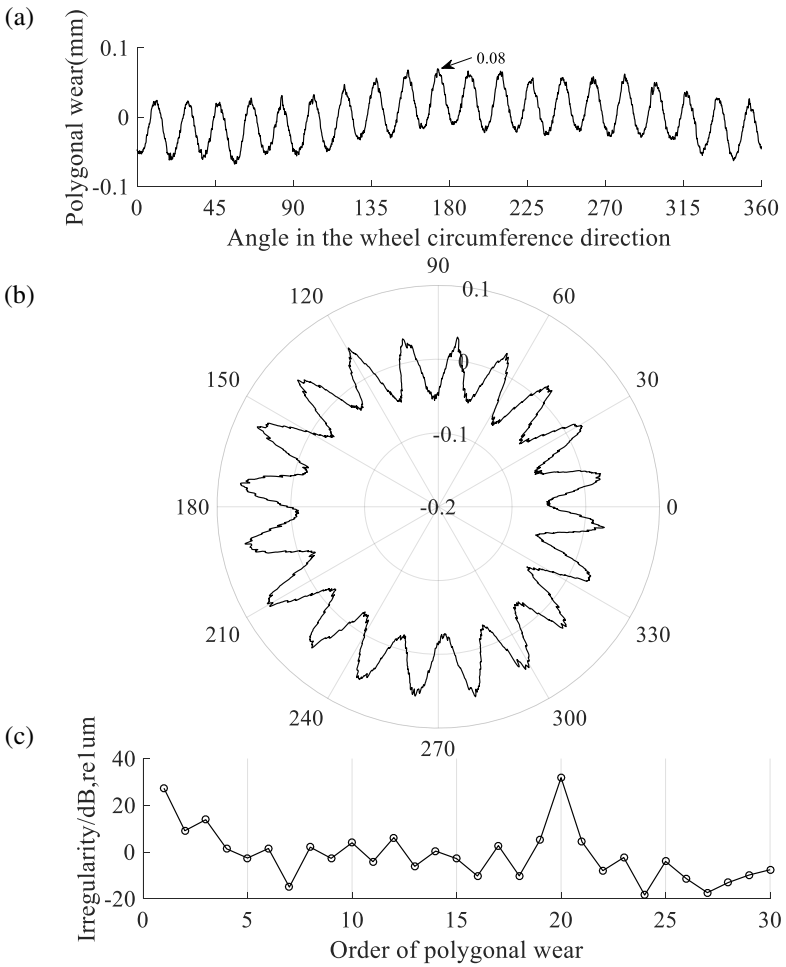

Figure 6 Measurement of polygonal wear on the wheel.

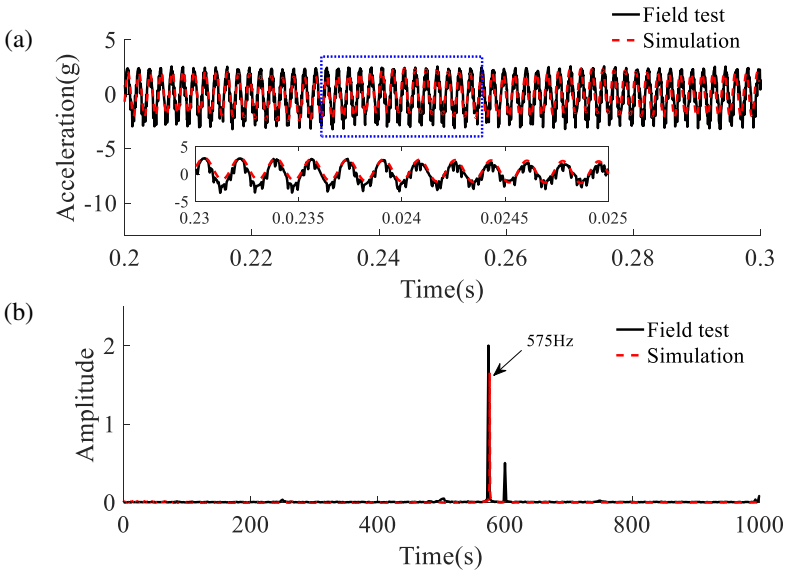

Figure 7 Comparison of results obtained by the field test and the simulation at 300 km/h. (a) Time histories of vibration acceleration of the bogie frame and (b) frequency spectrum of vibration acceleration of the bogie frame.

At a vehicle running speed of 300 km/h, the excitation frequency of 20th order polygonal wear is

576 Hz. Figure 7 (b) shows the frequency spectrum of the vibration acceleration of the bogie frame. It is clear that vibration of the bogie frame is dominated by 20th order polygonal wear. Based on analysis of the frequency and power of the spectrum results, we can conclude that the dynamic simulations of polygonal wear align well the experimental results in the context of this study.

Figure 8 shows the axle-box results obtained by numerical simulation and field testing at a speed of 300 km/h. It can be seen from Figure 8 (a) that the vibration of the axle-box acquired from test data is larger than the theoretical result. The primary reason for this is that due to the limitations of the modelling method and computational efficiency, the simulation omits some stiffness components, damping elements, the flexible deformation of components and the friction effects of the vehicle. Nevertheless, the fundamental dynamic features in the simulation agree suitably well with the experimental results. In Figure 8 (b), there is clear alignment of the dominant frequency peak in the axle-box accelerations in both the numerical simulations and the field test data; the peak is a result of 20th order polygonal wear.

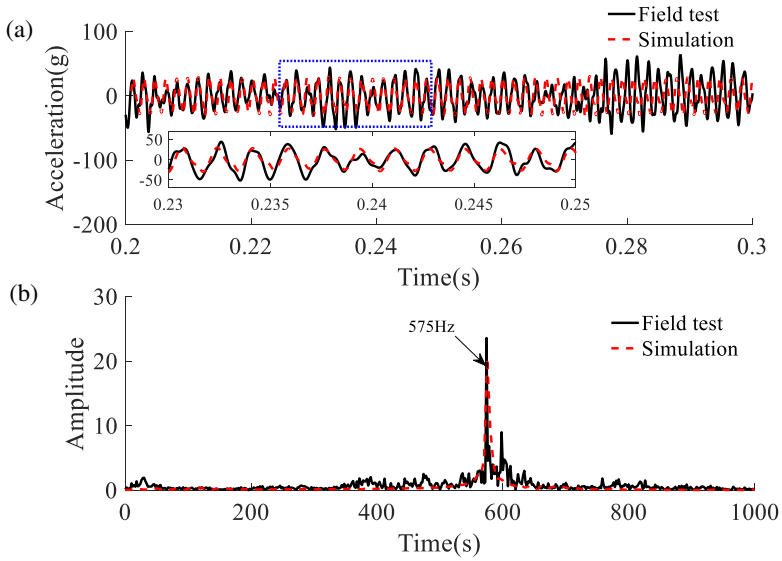

Figure 8 Comparison of results obtained by field test and simulation at 300 km/h. (a) Time histories of vibration acceleration of the axle-box and (b) frequency spectrum of vibration acceleration of the axle-box.

3.2 Vehicle system dynamics with and without an axle-box bearing model

In order to investigate the effect of inclusion of an axle-box bearing model on the vehicle system dynamics when excited by wheel polygonal wear, numerical simulations have been performed at a running speed 300 km/h. Once again, the predominant 20th order wheel polygonal wear pattern is applied, with an amplitude of 0.01 mm and no phase difference between the two wheels of a wheelset. The vertical vibration of the wheelset and bogie frame are illustrated in Figure 9 and Figure 10, respectively. The vertical direction is plotted as wheel polygonal wear predominantly influences vertical vibrations [12]. It can be seen that the axle-box bearing has little effect on the vibration of wheelset or bogie frame. The vibration of both wheelset and bogie frame are dominated by the 20th order polygonal wear, with an oscillation period of 1.734ms. The vertical vibration

acceleration of the carbody has a similar characteristic to the bogie frame, and hence is not presented here. The standard deviation (Std) of the wheelset vertical vibration is 3.85g and 3.77g with and without the axle-box bearing; the Std of the bogie frame vertical vibration is 0.285g and 0.281g with and without the axle-box bearing, respectively. Hence, in response to polygonal wear excitation, the wheel-rail interaction dominates the vibration of the vehicle components but the axle-box bearing has little effect.

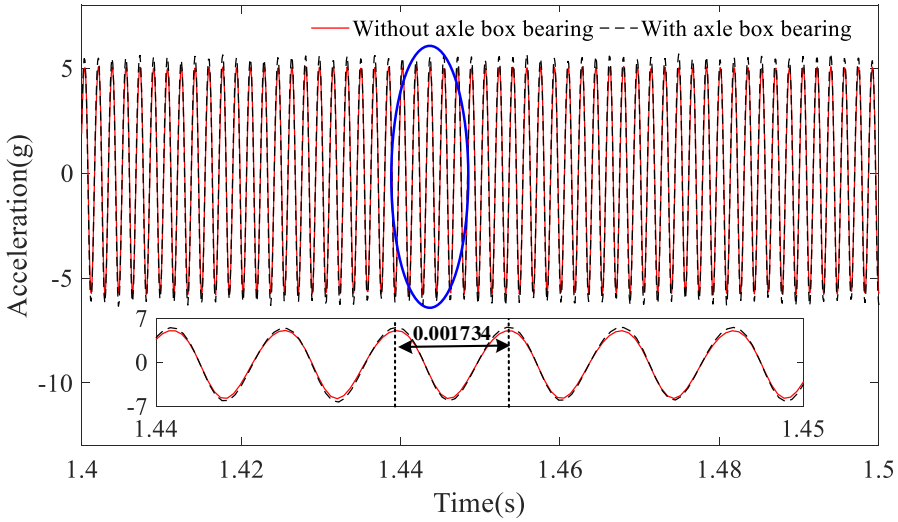

Figure 9 Vertical vibration acceleration of a wheelset excited by wheel polygonal wear.

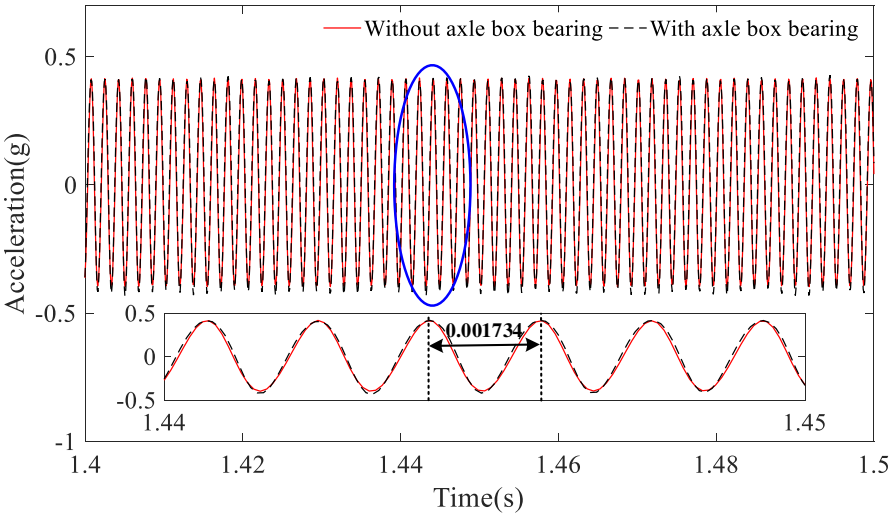

Figure 10 Vertical vibration acceleration of the bogie frame excited by wheel polygonal wear.

3.3 Influence of wear amplitude and vehicle running speed

The main advantage of the developed dynamic model as compared with previous studies is that it considers the coupling effects between the vehicle components and the axle-box bearing. To study the bearing's dynamic performance under polygonal wear, numerical simulations have been performed. The vehicle was run on straight track at a speed of 300 km/h, both wheels of the lead wheelset have a 20^{th} order polygonal wear pattern as defined in Figure 6, with no phase difference

between the wheels. Additionally, for comparative purposes, numerical simulations with non-polygonal wheels have also been performed.

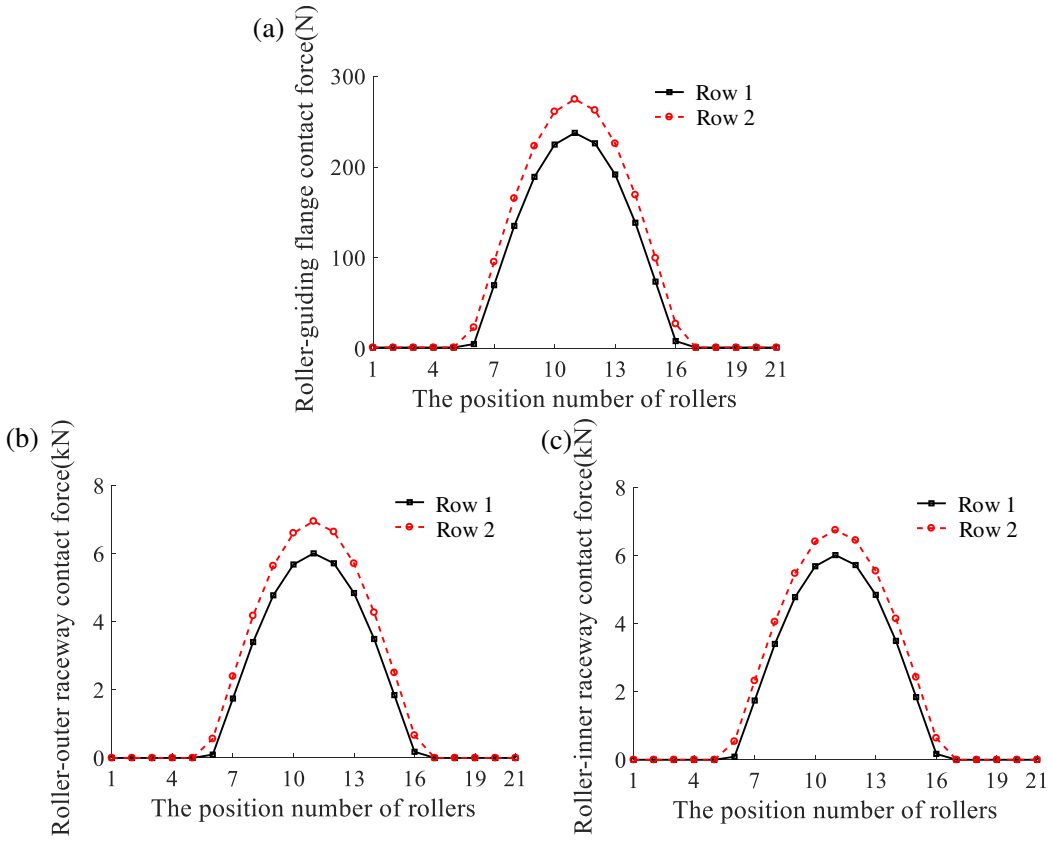

Figure 11 Contact forces of axle-box bearing. (a) Contact force of roller-guiding flange, (b) contact force of roller-outer raceway force, and (c) contact force of roller-inner raceway.

Figure 11 illustrates the contact forces of the roller-guiding flange, roller-outer raceway and roller-inner raceway under the measured polygonal wear at 300 km/h. It can be seen that the roller contact force of row 1 is different to that of row 2, this is due to the axial movement between the inner and outer raceway. For reference, the rollers of row 1 and 2 are presented diagrammatically in Figure 3. Moreover, it can be seen that there are similar dynamic trends in the contact forces between roller and inner and outer raceway. The peak value of roller-inner and roller-outer raceway contact force is far greater than the roller-guiding flange contact force. In addition, the roller-inner and roller-outer raceway contact force is almost the same due to little influence of the roller centrifugal forces. Hence, only the roller-outer raceway contact force is analysed below.

Figure 12 presents the results of the roller-outer ring raceway contact force, as obtained with and without polygonal wear, at a speed of 300 km/h. Figure 12 (a) shows the time histories of contact force between a roller and the outer-ring raceway and Figure 12 (b) shows this maximum force for each roller at the time identified in Figure 12 (a). Considering Figure 12 (a), it is clear that only part of the rollers bearing load is due to the applied axial and radial force. In addition, compared to the results obtained in the no-wear case, the contact force on each roller under polygonal wear is higher. It can be seen from Figure 12 (b) that the roller has both contact and non-contact regions in one cycle. Moreover, the results indicate that the contact force include high frequency oscillations caused by the polygonal wear. Compared with the results obtained in the no-wear case, the maximum amplitude of the roller-outer raceway contact force is increased by approximately 26%.

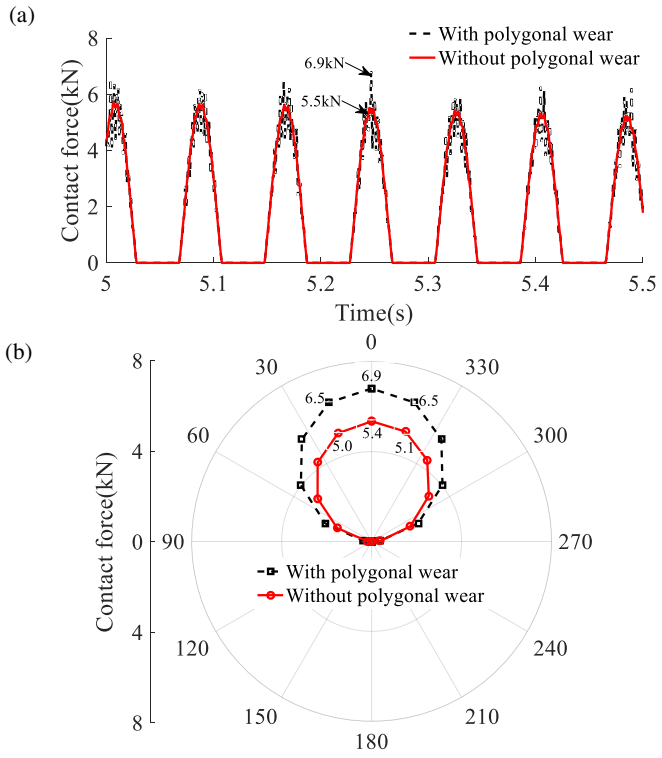

Figure 12 Comparison of the results obtained by simulation at 300 km/h. (a) Roller-outer-ring raceway contact force in the polar coordinate system and (b) time histories of the roller-outer-ring raceway contact force.

From the above analysis, it can be concluded that as the vibration of the axle-box is directly influenced by wheel-rail forces, polygonal wear has a significant impact on the dynamic forces within the axle-box bearing itself. Hence the observed change in the roller-outer ring raceway contact force is mainly due to the vibration of the wheelset induced by the fluctuations in the wheel-rail forces due to polygonal wear.

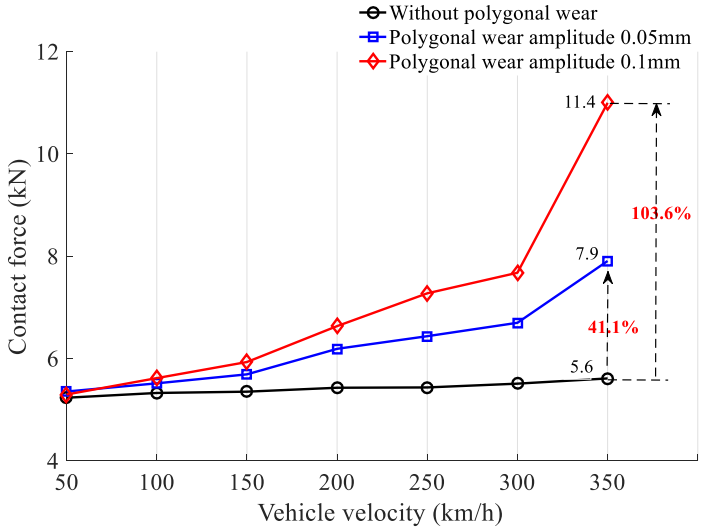

Figure 13 Maximum amplitude of roller-outer raceway contact force.

The idealised 20th order polygonal wear model has been adopted to investigate the effects of polygonal wear upon the axle-box bearing in detail. The maximum contact force considering the effects of polygonal wear amplitude and vehicle velocity is illustrated in Figure 13.

When the wheel has no defects, the contact force on the axle-box bearing is almost independent of vehicle-running speed. This is due to the fact that the applied axial and radial load on the bearing remains almost constant. It can be deduced that in the low-speed range of $V < 150$ km/h, the amplitude change of the dynamic contact force caused by polygonal wear is very small. However, the influence of polygonal wear increases sharply in the range of $V > 300$ km/h. When the polygonal wear amplitude changes from 0 to 0.1 mm, the contact force increases by approximately 103.6% at a speed of 350 km/h. Moreover, when the vehicle's running speed varies from 50 to 350 km/h, the contact force increases by 115.1% due to polygonal wear with an amplitude of 0.1 mm. Hence, the roller's contact force is directly affected by polygonal wear, especially when the vehicle runs at high speed.

3.4 Influence of the order of wheel polygonal wear

Figure 14 illustrate the influence of low and high orders of polygonal wear on the bearing contact forces at a speed of 300 km/h. The results are presented for 0.1mm polygonal wear amplitude on both wheels of the wheelset and the order ranges from 1 to 4 and 17 to 21, which often occur under normal train operations as described in the field measurement results.

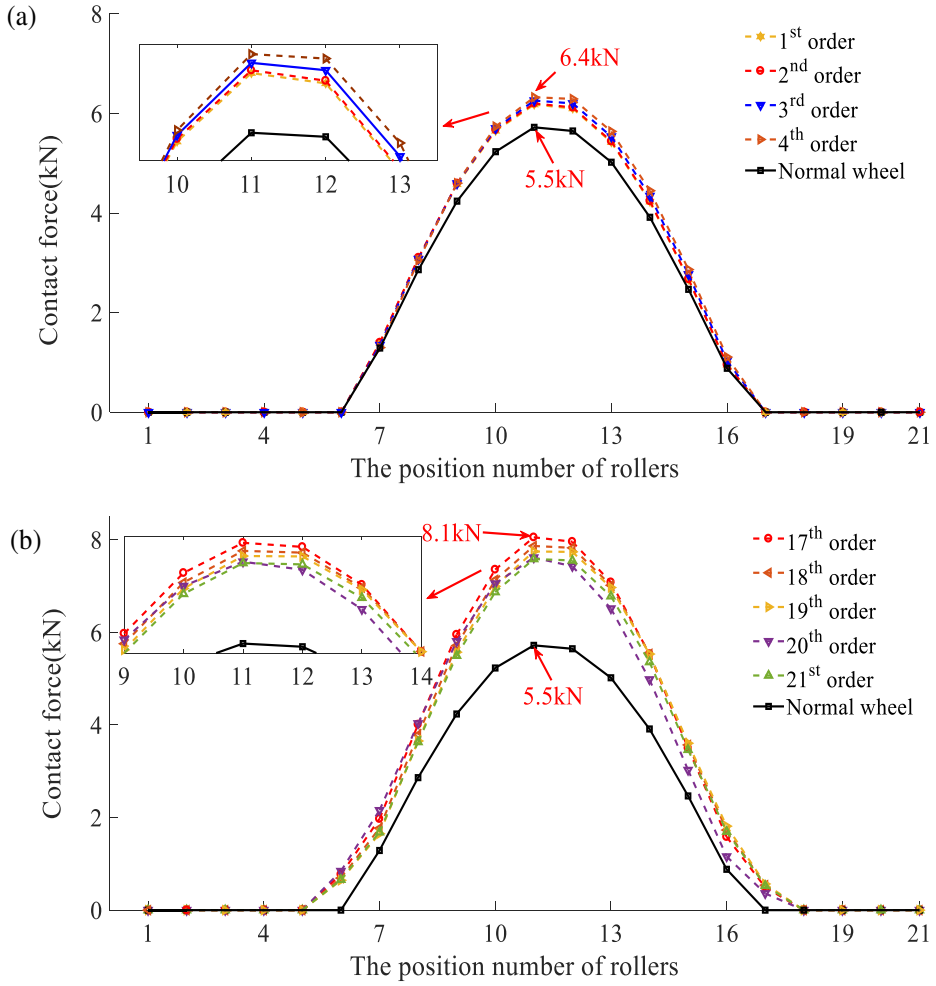

Figure 14 The contact force between the roller and outer raceway under the effects of (a) low order and (b) high order harmonic of wheel polygon wear.

When comparing a wheel with lower order polygonal wear geometry with that of a normal wheel

with no wear, then the maximum amplitude of the contact force is 6.4 kN, an increase of 16.4%. Moreover, it can be seen that the contact force offers little variation within a harmonic order ranging from 1 to 4. When considering higher 17^{th} order polygonal wear, the peak value of the contact force reaches 8.1 kN, an increase of 47.3% over a normal wheel. Similarly, the maximum amplitude of contact force changes little when the order increases from 17 to 21. However, the high order wheel polygonal wear has greater influence on the contact force than the lower order due to the higher wheel-rail forces. Therefore, the influence of high order wheel polygonal wear on TRBs of high-speed train should be considered in regards to bearing design, operation and maintenance.

4 Conclusions

To investigate the effects of wheel-polygonal wear upon a bearing's dynamic performance, a new vehicle-track coupled dynamics model that considers the axle-box bearing dynamics itself is developed in this study. The model couples the movements of the vehicle-track system with those of the axle-box via the axle-box bearing subsystem. Moreover, field tests are employed to validate the developed model and good agreement has been demonstrated. Based on the proposed model, the dynamic performance of the axle-box bearing under wheel polygonal wear can be analysed and discussed.

Comprehensive theoretical and experimental analyses of the effects of 20^{th} order polygonal-wheel wear upon the axle-box bearings of high-speed trains has been performed. The theoretical analysis indicates that polygonal wear significantly affects the roller-outer ring raceway contact force when the vehicle runs at higher speeds. When the amplitude of the polygonal wear reaches 0.1 mm, the maximum amplitude of the contact force is 11.4 kN at 350 km/h, representing an increase of 103.6% over results obtained without the presence of polygonal wear. In addition, high order wheel polygonal wear (17^{th} to 21^{st} order) has a more significant influence than low order (1^{st} to 4^{th} order) on axle-box bearing forces. Therefore, it is necessary to consider the effects of wheel-polygonal wear, especially high orders, when assessing the dynamic behaviour of the axle-box bearing of a high-speed train.

The developed dynamic model can also be used to investigate the effects of other wheel defects upon the dynamic performance of an axle-box bearing, which is a subject of future research work. In the proposed model, the friction between the internal components of bearing are ignored, and all bearing rollers have the same angular motion. The friction and angular vibration of each roller is likely to have some dynamic contribution to its dynamic forces, this forms a further aspect that will be investigated in future studies. Moreover, the flexible deformation of the bogie components and its effects on the axle-box bearing should also be considered in subsequent analysis.

5 Acknowledgments

The first author thanks the support of the China Scholarship Council.

6 Funding

The author(s) is grateful for the financial support provided by the National Key Research and Development Program of China (Grant No 2016YFB1200401-102B), State Key Laboratory of Traction Power, Southwest Jiaotong University (No.2016 TPL_T04) and the National Natural Science Foundation of China (Grant No. 51475391).

7 REFERENCES

1. S. Iwnicki. Handbook of railway vehicle dynamics. Boca Raton, FL: CRC Press; 2006.

2. A. Johansson, Out-of-round railway wheels – assessment of wheel tread irregularities in train traffic. J Sound Vib 2006; 293 (3): 795–806.

3. A. Ekberg, E. Kabo, Fatigue of railway wheels and rails under rolling contact and thermal loading—an overview. Wear 2005; 258 (7):1288–1300.

4. J.C.O. Nielsen, R. Lundén, A. Johansson, et al., Train-track interaction and mechanisms of irregular wear on wheel and rail surfaces. Veh Syst Dyn 2003; 40(1-3): 3-54.

5. J.C.O. Nielsen, A. Johansson, Out-of-round railway wheels-a literature survey. Proc IMechE, Part F: J Rail and Rapid Transit 2000; 214 (2): 79–91.

6. A. Johansson, J.C.O. Nielsen, Out-of-round railway wheels—wheel-rail contact forces and track response derived from field tests and numerical simulations. Proc IMechE, Part F: J Rail and Rapid Transit 2003; 217 (2): 135–146.

7. W.M. Zhai, Q.C. Wang, Z.W. Lu, et al., Dynamic effects of vehicles on tracks in the case of raising train speeds. Proc IMechE, Part F: J Rail and Rapid Transit 2001; 215 (2): 125–135.

8. X.Y. Liu, W.M. Zhai, Analysis of vertical dynamic wheel/rail interaction caused by polygonal wheels on high-speed trains. Wear 2014; 314 (1-2) 282–290.

9. P. Meinke, S. Meinke, Polygonalization of wheel treads caused by static and dynamic imbalances. J Sound Vib 1999;5 (11): 979–986.

10. Z.W. Wang, G.M. Ming, W.H. Zhang, et al. Effects of polygonal wear of wheels on the dynamic performance of the gearbox housing of a high-speed train. Proc IMechE, Part F: J Rail and Rapid Transit 2018; 232 (6): 1852-1863.

11. Wang ZW, Cheng Y, Mei GM, et al. Torsional vibration analysis of the gear transmission system of high-speed trains with wheel defects. Proc IMechE, Part F: J Rail and Rapid Transit 2019 DOI: 10.1177/0954409719833791.

12. X.W. Wu, S. Rakheja, S. Qu, et al., Dynamic responses of a high-speed railway car due to wheel polygonalisation. Veh Syst Dyn 2015; 53 (11): 1535–1554.

13. X.W. Wu, S. Rakheja, A.K.W. Ahmed, et al., Influence of a flexible wheelset on the dynamic responses of a high-speed railway car due to a wheel flat. Proc IMechE, Part F: J Rail and Rapid Transit 2017; 232(4): 1033-1048.

14. A. Palmgren, Ball and Roller Bearing Engineering, Philadelphia: SKF Industries Inc., Vol. 1, 1959.

15. A.B. Jones, A General Theory for Elastically Constrained Ball and Radial Roller Bearings under Arbitrary Load and Speed Conditions, J Fluids Eng 1960; 82 (2): 309–320.

16. T.A. Harris, Rolling Bearing Analysis, second ed., John Wiley &Sons, New York, 1984.

17. S. Andréason, Load distribution in a taper roller bearing arrangement considering misalignment. Tribology 1973; 6 (3): 84–92.
18. J.Y. Liu, Analysis of tapered roller bearings considering high speed and combined loading. J Tribol 1976; 98 (4): 564–572.
19. L. Houpert, An enhanced study of the load–displacement relationships for rolling element bearings. J Tribol 2014; 136 (1): 011105.
20. J. Liu, Y.M. Shao, X.M. Qin. Dynamic simulation for a tapered roller bearing considering a localized surface fault on the rib of the inner race. Proc IMechE Part K: J Multi-body Dynamics 2017; 231(4): 670-683.
21. Z.W. Wang, W.H. Zhang, Z.H. Yin, et al. Effect of vehicle vibration environment of high speed train on dynamic performance of axle box bearing. Veh Syst Dyn 2018; DOI: 10.1080/00423114.2018.1473615.
22. W.M. Zhai, X. Sun, A detailed model for investigating vertical interaction between railway vehicle and track. Veh Syst Dyn 1994; 23 (sup1): 603–615.
23. Z.G. Chen, W.M Zhai, K.Y. Wang, Dynamic investigation of a locomotive with effect of gear transmissions under tractive conditions. J Sound Vib 2017; 408 (10): 220–233.
24. D.W. Barke, W.K. Chiu, A review of the effects of out-of-round wheels on track and vehicle components. Proc IMechE, Part F: J Rail and Rapid Transit 2005; 219 (3):151–175.
25. W.M Zhai, K.Y. Wang, C.B. Cai, Fundamentals of vehicle–track coupled dynamics. Veh. Syst. Dyn 2009; 47 (11): 1349–1376.
26. W. Zhai, Z. Cai, Dynamic interaction between a lumped mass vehicle and a discretely supported continuous rail track. Comput. Struct 1997; 63 (5) :987–997.
27. Z.Y. Shen, J.K. Hedrick, J.A. Elkins, A comparison of alternative creep force models for rail vehicle dynamic analysis, Veh Syst Dyn 1983; 12(1-3): 79–83.
28. J.J. Kalker, Three-dimensional elastic bodies in rolling contact, Springer Science & Business Media 2 (2013).
29. G. Chen, W.M. Zhai, A new wheel/rail spatially dynamic coupling model and its verification, Veh Syst Dyn 2004; 41(4): 301–322.
30. W.M Zhai, H. Xia, C.B. Cai, et al. High-speed train-track-bridge dynamic interactions - Part I: theoretical model and numerical simulation, International Journal of Rail Transportation 2013; 1(1-2): 3-24.
31. J.W. Luo, T.Y. Luo. Calculation and application of rolling bearing, Beijing: China Ma-chine Press; 2009. in Chinese.
32. L.H. Yang, T.F. Xu, H.L. Xu, et al. Mechanical behavior of double-row tapered roller bearing under combined external loads and angular misalignment. International Journal of Mechanical Sciences 2018; 142-143: 561-574.
33. W.H. Zhang, Dynamics of coupled systems in high-speed trains: theory and practice. Beijing: Science press, 2013.